

# Markovian Jump Linear Systems-based filtering for Visual and GPS Aided Inertial Navigation System

Roberto S. Inoue<sup>1</sup> Vitor Guizilini<sup>2</sup> Marco H. Terra<sup>3</sup> Fabio Ramos<sup>2</sup>

**Abstract**— Visual-Inertial SLAM methods have become a very important technology for several applications in robotics. This kind of approach usually is composed by sensors as rate gyros, accelerometers and monocular cameras. Magnetometers and GPS modules generally used for outdoors are absent in the SLAM system observation, since the magnetometer measurements deteriorate in the presence of ferromagnetic materials and the GPS module signals are unavailable indoors or in urban environments. In order to make use of all these sensors, we propose Markovian jump linear systems (MJLS) to model the modes of operation of the navigation system based on available sensors and their reliability. An extended Kalman filter for MJLS fuses the sensor data and estimates the motion using the best mode of operation for each particular time instant. Experimental results are presented to show the effectiveness of the proposed method, in situations that would pose a challenge for standard data fusion techniques.

## I. INTRODUCTION

Visual simultaneous localization and mapping (VSLAM) has attracted attention for several applications in robotics lately, see [1], [2], [3], [4], [5] for some examples. This method consists in estimating from a stream of images the camera pose and environment model during navigation. Based on the way that VSLAM extracts information from the image [6], [7], [8], it can be classified as a featured-based method [9] or a direct method [10]. Featured-based methods use only information of the feature extraction process to obtain pose estimates and the 3D model, which can be arguably considered a limitation. However, it has a low computational cost, which is important for real-time applications, and that justifies the larger number of works using this method in mobile phones [11], [12], [13]. Direct methods, on the

other hand, use the entire array of image information to obtain pose estimates and the 3D model. Because of that, they have a high computational cost and are usually implemented on computers with GPU support. In mobile phones, recently [8] managed to use a direct approach for semi-dense depth maps of internal environments in augmented reality applications.

Additionally, VSLAM from a monocular camera has a scale ambiguity that limits its use in certain applications [14]. To overcome this issue, the technique called Visual-Inertial SLAM, that is VSLAM aided by an inertial navigation system (INS), has been widely used. This technique consists in fusing VSLAM with rate gyro and accelerometer information, usually using an extended Kalman filter [12], [15], [16]. Sensors such as magnetometers and GPS modules have not been used indoors [13], since magnetometer measurements deteriorate in the presence of ferromagnetic materials and GPS signals becomes unavailable indoors or in urban environments. However, these sensors have been successfully used for Unmanned Aerial Vehicle localization in outdoors tasks, since they provide absolute measurements which eliminate the drift in pose estimation [17]. That motivates the use of these sensors in outdoors SLAM approaches, such as in [18], [19].

The availability and reliability of this sensor in a filtering system could be modeled as a MJLS, which is a particular class of variant systems in random time. For example, in [20], [21] the authors presented a Kalman filter for MJLS to fuse four inertial sensors and three encoders from one exoskeleton's leg. A criterion based on the norm of the measured acceleration was established in order to select the best mode of operation. Results showed in [21] demonstrated that the MJLS-based KF outperformed the commonly used KF. Others applications of Kalman filter for MJLS can be seen in [22], [23], [24], [25], [26].

Taking into account this scenario, this paper proposes the use of MJLS to model the modes of operation of a navigation system based on sensors available and their reliability. The system is composed of an IMU, a monocular camera and a GPS module. A MJLS-based EKF fuses sensor data and estimates motion, using the best mode of operation for that time instant, what is an improvement over the standard Kalman filter implementation, that uses information from all sensors simultaneously. This ability is of utmost importance in robust long-term navigation, since the introduction of erroneous sensor

\*This work was supported by grants #2015/18085-8, #2014/08432-0 and #2014/50851-0, Sao Paulo Research Foundation (FAPESP) and grant #484095/2013-7 and #465755/2014-3 Brazilian National Council for Scientific and Technological Development (CNPq), and by the Faculty of Engineering and Information Technologies, The University of Sydney, under the Faculty Research Cluster Program.

<sup>1</sup>Roberto S. Inoue is with Department of Electrical Engineering, Federal University of São Carlos at São Carlos, São Paulo, Brazil and also as Visiting Research at School of Information Technologies, The University of Sydney, Australia. [rsinoue@ufscar.br](mailto:rsinoue@ufscar.br) <sup>2</sup>Vitor Guizilini and Fabio Ramos are with School of Information Technologies, The University of Sydney, Australia. [vitor.guizilini@sydney.edu.au](mailto:vitor.guizilini@sydney.edu.au); [fabio.ramos@sydney.edu.au](mailto:fabio.ramos@sydney.edu.au) Marco H. Terra is with Department of Electrical Engineering, University of São Paulo at São Carlos, São Paulo, Brazil. [terra@sc.usp.br](mailto:terra@sc.usp.br)

data can easily compromise localization estimates, and by extension other modules that rely on such information (i.e. mapping, path planning, collision avoidance).

This paper is organized as follows: In Section II the development of the MJLS for the Visual and GPS aided INS problem is presented. In Section III the estimate of the position scale of VSLAM, along with the availability and reliability of the sensors, are defined and the MJLS-based EKF algorithm is introduced. In Sections IV and V we present and discuss experimental results, before proving conclusions that should guide future work.

## II. MARKOVIAN ESTIMATION SYSTEM

In this section we present a MJLS for the Visual and GPS aided INS problem, also referred in this paper as Markovian Estimation System (MES), see Fig. 1. The system is composed of an IMU, a monocular camera and a GPS module. The IMU consists of a three-axis rate gyro, a three-axis accelerometer and a three-axis magnetometer, measuring respectively angular velocity, linear acceleration and magnetic field measurement. The monocular camera provides data for a VSLAM algorithm that outputs orientation, position and a 3D model of where it is currently located. Finally, the GPS module provides the outdoor location information.

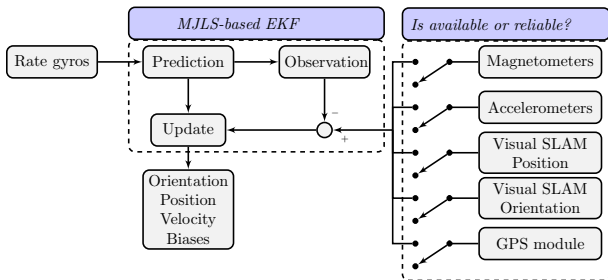


Fig. 1. Motion estimation system diagram.

The MJLSs are proposed as a way to model the modes of operation or the Markov state of the navigation system based on the availability and reliability of the sensors that can be observed. Once the Markov state is selected, the MJLS-based EKF fuses sensor data and estimates orientation, position and velocity of the platform, along with biases of the inertial sensors using the best mode of operation for that time instant.

The navigation system frames are shown in Fig. 2, where  $\{\mathcal{G}\}$  is the Global frame,  $\{\mathcal{L}\}$  is the Local frame,  $\{\mathcal{I}\}$  is the IMU frame,  $\{\mathcal{C}\}$  is the Camera frame and  $\{\mathcal{A}\}$  is the GPS module frame. The spatial transformations among the sensors and the Local frame  ${}^{\mathcal{L}}T$ ,  ${}^{\mathcal{L}}T$  and  ${}^{\mathcal{L}}T$  are considered known and constant. The orientation of the Global frame  $\{\mathcal{G}\}$  in the Local frame  $\{\mathcal{L}\}$  is represented by a unit quaternion  $q = [q_0 \ q_1 \ i \ q_2 \ j \ q_3 \ k]^T$ , where  $q_0, q_1, q_2$  and  $q_3$  are scalar values.

The position and velocity of  $\{\mathcal{L}\}$  in  $\{\mathcal{G}\}$  are represented by  ${}^{\mathcal{G}}\mathbf{p}$  and  ${}^{\mathcal{G}}\mathbf{v}$ , respectively, and the rate gyro

and accelerometer biases are described by  $\mathbf{b}_g$  and  $\mathbf{b}_a$ , respectively.

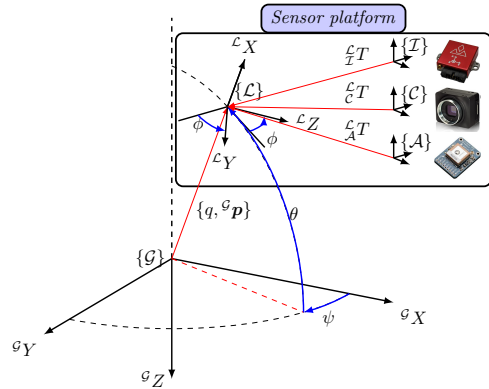


Fig. 2. Motion system frames.

In the next sections, we are going to present the motion error model, the measurement model and MJLSs for the problem described in this section.

### A. Motion error model

In this work, the motion model is established as an error state-space system in Section II-C. For this purpose, we show below the error motion equations of the system presented in Fig. 1. For more details of error models, please see [16], [27].

First, the error between the actual quaternion  $q$  and the estimated quaternion  $\hat{q}$  is defined as an incremental quaternion  $\delta q$  as shown below:

$$\delta q = \begin{bmatrix} \delta q_0 \\ \delta \mathbf{q} \end{bmatrix} = \begin{bmatrix} \cos\left(\frac{\delta e}{2}\right) \\ \sin\left(\frac{\delta e}{2}\right) \mathbf{u} \end{bmatrix} \approx \begin{bmatrix} 1 \\ \frac{1}{2}\delta \mathbf{e} \end{bmatrix}, \quad (1)$$

where  $\delta q_0$  is a scalar quantity,  $\delta \mathbf{q}$  is a vector,  $\mathbf{u}$  is the rotation axis and  $\delta e$  is the rotation angle, and  $\delta \mathbf{e}$  is the orientation error vector that has direction of  $\mathbf{u}$  and magnitude of  $\delta e$ .

Using the approximation (1), it is possible to write the derivative of the orientation error vector as:

$$\delta \dot{\mathbf{e}} \approx -\hat{\boldsymbol{\omega}} \times \delta \mathbf{e} - \delta \mathbf{b}_g - \mathbf{w}_g, \quad (2)$$

where  $\hat{\boldsymbol{\omega}} = \boldsymbol{\omega}_g - \hat{\mathbf{b}}_g$ ,  $\hat{\boldsymbol{\omega}}$  is the estimated angular velocity,  $\hat{\mathbf{b}}_g$  is the estimated rate gyro bias, and  $\delta \mathbf{b}_g = \mathbf{b}_g - \hat{\mathbf{b}}_g$ . The dynamic equation of  $\delta \mathbf{b}_g$  is given as:

$$\delta \dot{\mathbf{b}}_g = \Lambda_g \delta \mathbf{b}_g + \mathbf{w}_{b_g}, \quad (3)$$

where  $\Lambda_g$  is the correlation time matrix of the Gauss-Markov process.

The derivative of the linear velocity error using the approximation (1) is obtained as:

$${}^{\mathcal{G}}\delta \dot{\mathbf{v}} \approx -{}^{\mathcal{L}}\hat{R}^T [\hat{\mathbf{a}}^\times] \delta \mathbf{e} - {}^{\mathcal{L}}\hat{R}^T \delta \mathbf{b}_a - {}^{\mathcal{L}}\hat{R}^T \mathbf{w}_a, \quad (4)$$

where  ${}^{\mathcal{G}}\delta \mathbf{v} = {}^{\mathcal{G}}\mathbf{v} - {}^{\mathcal{G}}\hat{\mathbf{v}}$ ,  ${}^{\mathcal{G}}\hat{\mathbf{v}}$  is the estimated linear velocity,  $\delta \mathbf{b}_a = \mathbf{b}_a - \hat{\mathbf{b}}_a$  and  $\hat{\mathbf{b}}_a$  is the estimated accelerometer bias.

The dynamic equation of  $\delta \mathbf{b}_a$  is defined as:

$$\delta \dot{\mathbf{b}}_a = \Lambda_a \delta \mathbf{b}_a + \mathbf{w}_{b_a}, \quad (5)$$

where  $\Lambda_a$  is the correlation time matrix of the Gauss-Markov process.

And finally, we can define the position error derivative as

$${}^{\mathcal{G}}\delta \dot{\mathbf{p}} = {}^{\mathcal{G}}\delta \mathbf{v}. \quad (6)$$

where  ${}^{\mathcal{G}}\delta \mathbf{p} = {}^{\mathcal{G}}\mathbf{p} - {}^{\mathcal{G}}\hat{\mathbf{p}}$  and  ${}^{\mathcal{G}}\hat{\mathbf{p}}$  is the estimated position. The motion error equations obtained in this section are going to be used in the Section II-C in order to obtain the error Markovian state-space system.

### B. Measurement models

The error between the actual and estimated magnetometer measurement  $\widetilde{\mathbf{m}}_m = \mathbf{m}_m - \widehat{\mathbf{m}}_m$ , using the approximation (1) and following the steps shown in [27], can be written as:

$$\widetilde{\mathbf{m}}_m \approx \left[ \frac{\mathcal{L}}{\mathcal{G}} \widehat{R}^{\mathcal{G}} \mathbf{m}_e^{\times} \right] \delta \mathbf{e} + \mathbf{v}_m, \quad (7)$$

where  ${}^{\mathcal{G}}\mathbf{m}_e$  is the magnitude vector of Earth's magnetic field and  $\mathbf{v}_m$  is Gaussian white noise.

In order to observe the orientation of VSLAM, its quaternion  $q^{\text{VSO}}$  is converted to a magnetometer measurement in the following way:

$$\mathbf{m}_m^{\text{VSO}} = \frac{\mathcal{L}}{\mathcal{G}} \bar{R}^{\mathcal{G}} \mathbf{m}_e + \mathbf{v}_m^{\text{VSO}}, \quad (8)$$

where  $\frac{\mathcal{L}}{\mathcal{G}} \bar{R}$  is the rotation matrix in function of  $q^{\text{VSO}}$ , and  $\mathbf{v}_m^{\text{VSO}}$  is Gaussian white noise. Following the steps to obtain (7) for the Equation (8), we have:

$$\widetilde{\mathbf{m}}_m^{\text{VSO}} \approx \left[ \frac{\mathcal{L}}{\mathcal{G}} \widehat{R}^{\mathcal{G}} \mathbf{m}_e^{\times} \right] \delta \mathbf{e} + \mathbf{v}_m^{\text{VSO}}, \quad (9)$$

where  $\widetilde{\mathbf{m}}_m^{\text{VSO}} = \mathbf{m}_m^{\text{VSO}} - \widehat{\mathbf{m}}_m$ .

For orientation estimation purposes, we are interested in the gravity measurement in the Local frame  $\{\mathcal{L}\}$  [17]. This is possible when the rigid body has null dynamic acceleration. In this way, the error between the actual and estimated gravity measurement  $\widetilde{\mathbf{g}}_a = \mathbf{g}_a - \widehat{\mathbf{g}}_a$ , using the approximation (1) and following the steps shown in [27], is obtained as:

$$\widetilde{\mathbf{g}}_a \approx \left[ \left[ -\frac{\widehat{\mathcal{L}}}{\mathcal{G}} R(\widehat{q})^{\mathcal{G}} \mathbf{g}_e^{\times} \right] I_{3 \times 3} \right] \begin{bmatrix} \delta \mathbf{e} \\ \delta \mathbf{b}_a \end{bmatrix} + \mathbf{v}_a, \quad (10)$$

where  ${}^{\mathcal{G}}\mathbf{g}_e$  is the Earth's gravity vector and  $\mathbf{v}_a$  is Gaussian white noise.

The error between VSLAM position and the estimated position is modeled as:

$${}^{\mathcal{G}}\widetilde{\delta \mathbf{p}}^{\text{VSP}} = {}^{\mathcal{G}}\delta \mathbf{p} + \mathbf{v}_p^{\text{VSP}}, \quad (11)$$

and the error between the GPS position and the estimated position is modeled as:

$${}^{\mathcal{G}}\widetilde{\delta \mathbf{p}}^{\text{GP}} = {}^{\mathcal{G}}\delta \mathbf{p} + \mathbf{v}_p^{\text{GP}}. \quad (12)$$

### C. Error Markovian state-space system

In this section, we propose the MJLS for the Visual and GPS aided INS. All the modes of operation of the MJLS proposed in this work are defined in Table I. Combining the equations (2), (3), (4), (5) and (6) the error state-space model is obtained as:

$$\dot{\mathbf{x}} = \mathbf{A}\mathbf{x} + \mathbf{B}\mathbf{w}. \quad (13)$$

where  $\mathbf{x} = [\delta \mathbf{e}^T \quad \delta \mathbf{b}_g^T \quad {}^{\mathcal{G}}\delta \mathbf{v} \quad \delta \mathbf{b}_a^T \quad {}^{\mathcal{G}}\delta \mathbf{p}] \in \mathbb{R}^{15 \times 1}$  is the state that describes the motion system,  $\mathbf{w} = \left[ \mathbf{w}_g^T \quad \mathbf{w}_{b_g}^T \quad \mathbf{w}_a^T \quad \mathbf{w}_{b_a}^T \right]^T \in \mathbb{R}^{12 \times 1}$  is the Gaussian white noise vector with covariance matrix  $\mathbf{Q}$ , and:

$$\mathbf{A} = \begin{bmatrix} -[\widehat{\boldsymbol{\omega}}^{\times}] & -I_{3 \times 3} & 0_{3 \times 3} & 0_{3 \times 3} & 0_{3 \times 3} \\ 0_{3 \times 3} & \Lambda_g & 0_{3 \times 3} & 0_{3 \times 3} & 0_{3 \times 3} \\ -\frac{\mathcal{L}}{\mathcal{G}} \widehat{R}^T [\widehat{\mathbf{a}}^{\times}] & 0_{3 \times 3} & 0_{3 \times 3} & -\frac{\mathcal{L}}{\mathcal{G}} \widehat{R}^T & 0_{3 \times 3} \\ 0_{3 \times 3} & 0_{3 \times 3} & 0_{3 \times 3} & \Lambda_a & 0_{3 \times 3} \\ 0_{3 \times 3} & 0_{3 \times 3} & 0_{3 \times 3} & 0_{3 \times 3} & I_{3 \times 3} \end{bmatrix},$$

$$\mathbf{B} = \begin{bmatrix} -I_{3 \times 3} & 0_{3 \times 3} & 0_{3 \times 3} & 0_{3 \times 3} \\ 0_{3 \times 3} & I_{3 \times 3} & 0_{3 \times 3} & 0_{3 \times 3} \\ 0_{3 \times 3} & I_{3 \times 3} & -\frac{\mathcal{L}}{\mathcal{G}} \widehat{R}^T & 0_{3 \times 3} \\ 0_{3 \times 3} & 0_{3 \times 3} & 0_{3 \times 3} & I_{3 \times 3} \\ 0_{3 \times 3} & 0_{3 \times 3} & 0_{3 \times 3} & 0_{3 \times 3} \end{bmatrix}.$$

Using the equations (7), (9), (10), (11) and (12) the measurement model is written as:

$$\mathbf{z}_{\Theta} = \mathbf{C}_{\Theta} \mathbf{x} + \mathbf{v}_{\Theta}, \quad (14)$$

where  $\mathbf{z}_{\Theta} = [\mathbf{z}_{\Theta}^{1T} \quad \mathbf{z}_{\Theta}^{2T} \quad \mathbf{z}_{\Theta}^{3T}]^T \in \mathbb{R}^{9 \times 1}$  is the measurement error vector,  $\mathbf{v}_{\Theta} = [\mathbf{v}_{\Theta}^{1T} \quad \mathbf{v}_{\Theta}^{2T} \quad \mathbf{v}_{\Theta}^{3T}]^T \in \mathbb{R}^{9 \times 1}$  is the Gaussian white noise vector with covariance matrix  $R_{\Theta}$ , and:

$$\mathbf{C}_{\Theta} = \begin{bmatrix} C_{\Theta}^{11} & 0_{3 \times 3} & 0_{3 \times 3} & 0_{3 \times 3} & 0_{3 \times 3} \\ C_{\Theta}^{21} & 0_{3 \times 3} & 0_{3 \times 3} & C_{\Theta}^{24} & 0_{3 \times 3} \\ 0_{3 \times 3} & 0_{3 \times 3} & 0_{3 \times 3} & 0_{3 \times 3} & C_{\Theta}^{35} \end{bmatrix}.$$

$\mathbf{z}_{\Theta}^1, \mathbf{z}_{\Theta}^2, \mathbf{z}_{\Theta}^3, \mathbf{v}_{\Theta}^1, \mathbf{v}_{\Theta}^2, \mathbf{v}_{\Theta}^3, C_{\Theta}^{11}, C_{\Theta}^{21}, C_{\Theta}^{24}$  and  $C_{\Theta}^{35}$  are defined in accordance to the operation mode of the motion system as shown in Table I.

## III. IMPLEMENTATION

In this section we present the methods used to estimate the metric scale for the position of VSLAM, the guidelines to define if the sensor is available or reliable, which define the choice of the Markov mode established in Table I, and lastly the algorithm for MJLS-based EKF for the Visual and GPS aided INS problem.

### A. Scale estimation

Estimation of VSLAM scale consists of detecting the instants in which the platform is moving and comparing this displacement with a reference. The intervals in which the platform is moving are detected by analyzing the derivative of the velocity obtained by the VSLAM position. When the magnitude of the VSLAM velocity is larger than a specific threshold, we can compute the

TABLE I  
OPERATION MODES OF THE MJLS

Markov state ( $\Theta$ )	$\mathbf{z}_\Theta^1$	$\mathbf{z}_\Theta^2$	$\mathbf{z}_\Theta^3$	$\mathbf{v}_\Theta^1$	$\mathbf{v}_\Theta^2$	$\mathbf{v}_\Theta^3$	$C_\Theta^{11}$	$C_\Theta^{21}$	$C_\Theta^{24}$	$C_\Theta^{35}$
NS-G-NS	$0_{3 \times 3}$	$\bar{\mathbf{g}}_a$	$0_{3 \times 3}$	$0_{3 \times 3}$	$\mathbf{v}_a$	$0_{3 \times 3}$	$0_{3 \times 3}$	$-\left[\frac{\mathcal{L}}{\mathcal{G}} \hat{R}^{\mathcal{G}} \mathbf{g}_e^\times\right]$	$I_{3 \times 3}$	$0_{3 \times 3}$
VSO-G-NS	$\bar{\mathbf{m}}_m^{\text{VSO}}$	$\bar{\mathbf{g}}_a$	$0_{3 \times 3}$	$\mathbf{v}_m^{\text{VSO}}$	$\mathbf{v}_a$	$0_{3 \times 3}$	$\left[\frac{\mathcal{L}}{\mathcal{G}} \hat{R}^{\mathcal{G}} \mathbf{m}_e^\times\right]$	$-\left[\frac{\mathcal{L}}{\mathcal{G}} \hat{R}^{\mathcal{G}} \mathbf{g}_e^\times\right]$	$I_{3 \times 3}$	$0_{3 \times 3}$
VSO-G-VSP	$\bar{\mathbf{m}}_m^{\text{VSO}}$	$\bar{\mathbf{g}}_a$	$\mathcal{G}_{\delta \mathbf{p}}^{\text{VSP}}$	$\mathbf{v}_m^{\text{VSO}}$	$\mathbf{v}_a$	$\mathbf{v}_p^{\text{VSP}}$	$\left[\frac{\mathcal{L}}{\mathcal{G}} \hat{R}^{\mathcal{G}} \mathbf{m}_e^\times\right]$	$-\left[\frac{\mathcal{L}}{\mathcal{G}} \hat{R}^{\mathcal{G}} \mathbf{g}_e^\times\right]$	$I_{3 \times 3}$	$I_{3 \times 3}$
VSO-G-GP	$\bar{\mathbf{m}}_m^{\text{VSO}}$	$\bar{\mathbf{g}}_a$	$\mathcal{G}_{\delta \mathbf{p}}^{\text{GP}}$	$\mathbf{v}_m^{\text{VSO}}$	$\mathbf{v}_a$	$\mathbf{v}_p^{\text{GP}}$	$\left[\frac{\mathcal{L}}{\mathcal{G}} \hat{R}^{\mathcal{G}} \mathbf{m}_e^\times\right]$	$-\left[\frac{\mathcal{L}}{\mathcal{G}} \hat{R}^{\mathcal{G}} \mathbf{g}_e^\times\right]$	$I_{3 \times 3}$	$I_{3 \times 3}$
NS-M-G	$\bar{\mathbf{m}}_m$	$\bar{\mathbf{g}}_a$	$0_{3 \times 3}$	$\mathbf{v}_m$	$\mathbf{v}_a$	$0_{3 \times 3}$	$\left[\frac{\mathcal{L}}{\mathcal{G}} \hat{R}^{\mathcal{G}} \mathbf{m}_e^\times\right]$	$-\left[\frac{\mathcal{L}}{\mathcal{G}} \hat{R}^{\mathcal{G}} \mathbf{g}_e^\times\right]$	$I_{3 \times 3}$	$I_{3 \times 3}$
M-G-GP	$\bar{\mathbf{m}}_m$	$\bar{\mathbf{g}}_a$	$\mathcal{G}_{\delta \mathbf{p}}^{\text{GP}}$	$\mathbf{v}_m$	$\mathbf{v}_a$	$\mathbf{v}_p^{\text{GP}}$	$\left[\frac{\mathcal{L}}{\mathcal{G}} \hat{R}^{\mathcal{G}} \mathbf{m}_e^\times\right]$	$-\left[\frac{\mathcal{L}}{\mathcal{G}} \hat{R}^{\mathcal{G}} \mathbf{g}_e^\times\right]$	$I_{3 \times 3}$	$I_{3 \times 3}$
M-G-VSP	$\bar{\mathbf{m}}_m$	$\bar{\mathbf{g}}_a$	$\mathcal{G}_{\delta \mathbf{p}}^{\text{VSP}}$	$\mathbf{v}_m$	$\mathbf{v}_a$	$\mathbf{v}_p^{\text{VSP}}$	$\left[\frac{\mathcal{L}}{\mathcal{G}} \hat{R}^{\mathcal{G}} \mathbf{m}_e^\times\right]$	$-\left[\frac{\mathcal{L}}{\mathcal{G}} \hat{R}^{\mathcal{G}} \mathbf{g}_e^\times\right]$	$I_{3 \times 3}$	$I_{3 \times 3}$
NS-NS-NS	$0_{3 \times 3}$	$0_{3 \times 3}$	$0_{3 \times 3}$	$0_{3 \times 3}$	$0_{3 \times 3}$	$0_{3 \times 3}$	$0_{3 \times 3}$	$0_{3 \times 3}$	$0_{3 \times 3}$	$0_{3 \times 3}$
VSO-NS-NS	$\bar{\mathbf{m}}_m^{\text{VSO}}$	$0_{3 \times 3}$	$0_{3 \times 3}$	$\mathbf{v}_m^{\text{VSO}}$	$0_{3 \times 3}$	$0_{3 \times 3}$	$\left[\frac{\mathcal{L}}{\mathcal{G}} \hat{R}^{\mathcal{G}} \mathbf{m}_e^\times\right]$	$0_{3 \times 3}$	$0_{3 \times 3}$	$0_{3 \times 3}$
VSO-NS-VSP	$\bar{\mathbf{m}}_m^{\text{VSO}}$	$0_{3 \times 3}$	$\mathcal{G}_{\delta \mathbf{p}}^{\text{VSP}}$	$\mathbf{v}_m^{\text{VSO}}$	$0_{3 \times 3}$	$\mathbf{v}_p^{\text{VSP}}$	$\left[\frac{\mathcal{L}}{\mathcal{G}} \hat{R}^{\mathcal{G}} \mathbf{m}_e^\times\right]$	$0_{3 \times 3}$	$0_{3 \times 3}$	$I_{3 \times 3}$
VSO-NS-GP	$\bar{\mathbf{m}}_m^{\text{VSO}}$	$0_{3 \times 3}$	$\mathcal{G}_{\delta \mathbf{p}}^{\text{GP}}$	$\mathbf{v}_m^{\text{VSO}}$	$0_{3 \times 3}$	$\mathbf{v}_p^{\text{GP}}$	$\left[\frac{\mathcal{L}}{\mathcal{G}} \hat{R}^{\mathcal{G}} \mathbf{m}_e^\times\right]$	$0_{3 \times 3}$	$0_{3 \times 3}$	$I_{3 \times 3}$
M-NS-NS	$\bar{\mathbf{m}}_m$	$0_{3 \times 3}$	$0_{3 \times 3}$	$\mathbf{v}_m$	$0_{3 \times 3}$	$0_{3 \times 3}$	$\left[\frac{\mathcal{L}}{\mathcal{G}} \hat{R}^{\mathcal{G}} \mathbf{m}_e^\times\right]$	$0_{3 \times 3}$	$0_{3 \times 3}$	$I_{3 \times 3}$
M-NS-GP	$\bar{\mathbf{m}}_m$	$0_{3 \times 3}$	$\mathcal{G}_{\delta \mathbf{p}}^{\text{GP}}$	$\mathbf{v}_m$	$0_{3 \times 3}$	$\mathbf{v}_p^{\text{GP}}$	$\left[\frac{\mathcal{L}}{\mathcal{G}} \hat{R}^{\mathcal{G}} \mathbf{m}_e^\times\right]$	$0_{3 \times 3}$	$0_{3 \times 3}$	$I_{3 \times 3}$
M-NS-VSP	$\bar{\mathbf{m}}_m$	$0_{3 \times 3}$	$\mathcal{G}_{\delta \mathbf{p}}^{\text{VSP}}$	$\mathbf{v}_m$	$0_{3 \times 3}$	$\mathbf{v}_p^{\text{VSP}}$	$\left[\frac{\mathcal{L}}{\mathcal{G}} \hat{R}^{\mathcal{G}} \mathbf{m}_e^\times\right]$	$0_{3 \times 3}$	$0_{3 \times 3}$	$I_{3 \times 3}$

displacements of VSLAM  $\mathbf{d}^{\text{VSP}}$  and its reference  $\mathbf{d}^{\text{Ref}}$ . The scale metric is then estimated using a low-pass filter:

$$\hat{\lambda}_{k+1} = \alpha \hat{\lambda}_k + (1 - \alpha) \frac{\|\mathbf{d}^{\text{Ref}}\|}{\|\mathbf{d}^{\text{VSP}}\|} \quad (15)$$

where  $\alpha$  is a constant in the range of  $0 < \alpha < 1$ . After  $n$  iterations, the scale  $\hat{\lambda}_{k+1}$  is used in the VSLAM position and the Markov mode VSP of Table I is considered *true*.

### B. Available and reliable sensors

In this section we define availability and reliability of the sensors used in the MES, and according to them the Markov modes established in Table I are defined. As discussed in Section II-B, we are interested in measuring the accelerometer when the system has null dynamic acceleration. This situation occurs if the following condition is true:

$$\left| \left( \frac{\|\mathbf{a}_a\|}{\|\mathbf{g}_e\|} - 1 \right) \right| < \rho_a, \quad (16)$$

where  $\rho_a$  is a threshold value. The Markov mode G is considered *true* if the condition (16) is *true*. The magnetometer measurements deteriorates in the presence of ferromagnetic materials, so the magnetometer is assumed reliable if the following condition is true:

$$\left| \left( \frac{\|\mathbf{m}_m\|}{\|\mathbf{m}_e\|} - 1 \right) \right| < \rho_m, \quad (17)$$

where  $\rho_m$  is a threshold value. The Markov mode M is assumed *true* if the condition (17) is *true* and the Markov mode VSO is *false*. The Markov mode VSO is *true* if VSLAM orientation is available.

The Markov mode VSP is *true* if VSLAM position is available and the metric scale  $\hat{\lambda}$  has already been estimated by the scale estimation system shown in Section

III-A. The Markov mode VSP could be set as *false* if the following condition is true:

$$\|\mathcal{G}_{\mathbf{p}}^{\text{VSP}} - \mathcal{G}_{\mathbf{p}}^{\text{GP}}\| < \rho_p, \quad (18)$$

where  $\rho_p$  is a threshold value,  $\mathcal{G}_{\mathbf{p}}^{\text{VSP}}$  is the VSLAM position and  $\mathcal{G}_{\mathbf{p}}^{\text{GP}}$  is the GPS position. In the instants that condition (18) is *true* the VSLAM position is considered not reliable. Finally, the Markov mode GP is *true* if the position of the GPS module is available and the Markov mode VSP is *false*.

### C. MJLS-based EKF

The MJLS-based EKF here presented is based on a discrete-time system analysis. In this sense, (13) and (14) are discretized considering the sample time  $T$  as:

$$\begin{aligned} \mathbf{x}_{k+1} &= F_k \mathbf{x}_k + G_k \mathbf{w}_k, \\ \mathbf{z}_{\Theta,k} &= H_{\Theta,k} \mathbf{x}_k + \mathbf{v}_{\Theta,k}, \end{aligned} \quad (19)$$

where

$$F_k \simeq I + AT, \quad G_k \simeq BT^{\frac{1}{2}}, \quad H_{\Theta,k} = \frac{\partial \mathbf{z}_{\Theta}(\mathbf{x})}{\partial \mathbf{x}}.$$

Once the state  $\hat{\mathbf{x}}_{k+1|k+1}$  is estimated, it is necessary to update the orientation quaternion  $\hat{q}_{k+1|k+1}$  [27], this is done in the following way:

$$\hat{q}_{k+1|k+1} = \delta \hat{q}_{k+1|k+1} \otimes \hat{q}_{k+1|k},$$

where

$$\delta \hat{q}_{k+1|k+1} = \begin{bmatrix} \sqrt{1 + \delta \mathbf{e}_{k+1|k+1}^T \delta \mathbf{e}_{k+1|k+1}} \\ \delta \mathbf{e}_{k+1|k+1} \end{bmatrix},$$

or, if  $\delta \mathbf{e}_{k+1|k+1}^T \delta \mathbf{e}_{k+1|k+1} > 1$ :

$$\delta \hat{q}_{k+1|k+1} = \frac{1}{\sqrt{1 - \delta \mathbf{e}_{k+1|k+1}^T \delta \mathbf{e}_{k+1|k+1}}} \begin{bmatrix} 1 \\ \delta \mathbf{e}_{k+1|k+1} \end{bmatrix}. \quad (20)$$

The accelerometer and rate-gyro biases are respectively propagated as:

$$\widehat{\mathbf{b}}_{g,k+1|k} = T\Lambda_g \widehat{\mathbf{b}}_{g,k|k} + \widehat{\mathbf{b}}_{g,k|k}, \quad (21)$$

$$\widehat{\mathbf{b}}_{a,k+1|k} = T\Lambda_g \widehat{\mathbf{b}}_{a,k|k} + \widehat{\mathbf{b}}_{a,k|k}, \quad (22)$$

Using the measurement  $\omega_{g,k+1}$  and  $\widehat{\mathbf{b}}_{g,k+1|k}$ , we obtain the estimate of the new turn rate:

$$\widehat{\omega}_{k+1|k} = \omega_{g,k+1} - \widehat{\mathbf{b}}_{g,k+1|k}. \quad (23)$$

Using the measurement  $\mathbf{a}_{a,k+1}$  and  $\widehat{\mathbf{b}}_{a,k+1|k}$ , we obtain the estimate of the new accelerometer measurement:

$$\widehat{\mathbf{a}}_{k+1|k} = \mathbf{a}_{a,k+1} - \widehat{\mathbf{b}}_{a,k+1|k}. \quad (24)$$

The quaternion  $\widehat{q}_{k+1|k}$  is propagated as [17]:

$$\widehat{q}_{k+1|k} = \left( \cos(\|\bar{\omega}\|) I + \frac{\sin(\|\bar{\omega}\|)}{\|\bar{\omega}\|} \bar{\Omega} \right) \widehat{q}_{k|k}, \quad (25)$$

where  $\bar{\omega} = [\bar{\omega}_1 \ \bar{\omega}_2 \ \bar{\omega}_3]^T$  and

$$\bar{\Omega} = \begin{bmatrix} 0 & -\bar{\omega}_1 & -\bar{\omega}_2 & -\bar{\omega}_3 \\ \bar{\omega}_1 & 0 & -\bar{\omega}_2 & -\bar{\omega}_3 \\ \bar{\omega}_2 & \bar{\omega}_3 & 0 & -\bar{\omega}_1 \\ \bar{\omega}_3 & \bar{\omega}_2 & \bar{\omega}_1 & 0 \end{bmatrix} \quad (26)$$

$\bar{\omega}_1 = T\omega_{1,k+1|k}$ ,  $\bar{\omega}_2 = T\omega_{2,k+1|k}$ ,  $\bar{\omega}_3 = T\omega_{3,k+1|k}$ , and  $\widehat{\omega}_{k+1|k} = [\omega_{1,k+1|k} \ \omega_{2,k+1|k} \ \omega_{3,k+1|k}]^T$ . The linear velocity  ${}^g\widehat{\mathbf{v}}_{k+1|k}$  and position  ${}^g\widehat{\mathbf{p}}_{k+1|k}$  are propagated as:

$${}^g\widehat{\mathbf{v}}_{k+1|k} = \xi \widehat{R}^T \widehat{\mathbf{a}}_{k+1|k} + {}^g\mathbf{g}_e, \quad (27)$$

$${}^g\widehat{\mathbf{v}}_{k+1|k} = T{}^g\widehat{\mathbf{v}}_{k+1|k} dt + {}^g\widehat{\mathbf{v}}_{k|k}, \quad (28)$$

$${}^g\widehat{\mathbf{p}}_{k+1|k} = T{}^g\widehat{\mathbf{v}}_{k+1|k} dt + {}^g\widehat{\mathbf{p}}_{k|k}. \quad (29)$$

Finally, the EKF algorithm for the MJLS presented in Section II is depicted in Algorithm 1.

---

### Algorithm 1 MJLS-based EKF

---

// **Propagation:**

- 1: Reset error state  $\widehat{\mathbf{x}}_{k|k}$ .
- 2: Propagate biases using (21) and (22).
- 3: Correct velocities using (23) and (24).
- 4: Propagate the quaternion  $\widehat{q}_{k+1|k}$  using (25).
- 5: Propagate the linear velocity and position using (28) and (29), respectively.
- 6:  $P_{k+1|k} = F_k P_{k|k} F^T + G_k Q_k G_k^T$

// **Update:**

- 1: Determine the Markov mode  $\Theta$  using the reliable and available sensors, see Section III-B, and compute  $H_{\Theta,k}$  and  $R_{\Theta,k}$  based on Table I.
- 2:  $K_{k+1} = P_{k+1} H_{\Theta,k}^T (H_{\Theta,k} P_{k+1} H_{\Theta,k}^T + R_{\Theta,k})^{-1}$
- 3:  $\widehat{\mathbf{x}}_{k+1|k+1} = \widehat{\mathbf{x}}_{k+1|k} + K_{k+1} \mathbf{z}_{\Theta,k+1}$
- 4:  $P_{k+1|k+1} = (I - K_{k+1} H_{\Theta,k}) P_{k+1|k}$

// **Output:**

- 1: Obtain  $\delta \mathbf{e}_{k+1|k+1}$ ,  $\delta \mathbf{b}_{g,k+1|k+1}$ ,  ${}^g\delta \mathbf{v}_{k+1|k+1}$ ,  $\delta \mathbf{b}_{a,k+1|k+1}$ , and  ${}^g\delta \mathbf{p}_{k+1|k+1}$  from  $\widehat{\mathbf{x}}_{k+1|k+1}$ .
  - 2: Update the quaternion according to (20).
  - 3:  $\mathbf{b}_{g,k+1|k+1} = \mathbf{b}_{g,k+1|k} + \delta \mathbf{b}_{g,k+1|k+1}$
  - 4:  ${}^g\mathbf{v}_{k+1|k+1} = {}^g\mathbf{v}_{k+1|k} + {}^g\delta \mathbf{v}_{k+1|k+1}$
  - 5:  $\mathbf{b}_{a,k+1|k+1} = \mathbf{b}_{a,k+1|k} + \delta \mathbf{b}_{a,k+1|k+1}$
  - 6:  ${}^g\mathbf{p}_{k+1|k+1} = {}^g\mathbf{p}_{k+1|k} + {}^g\delta \mathbf{p}_{k+1|k+1}$
- 

## IV. EXPERIMENTAL RESULTS

Experimental results were obtained in a laptop with an Intel i7-3537U processor with 8 GB of RAM. The stream of images was obtained through a Point Grey Chameleon3 camera at 50 Hz with 1/2" 1.55mm IR MP fisheye lens. The VSLAM used was the Monocular ORB-SLAM2 [28] with 5000 features per image running at 10 Hz. The camera was calibrated using the Robot Operating System (ROS) package `camera_calibration`. The inertial data and GPS position were provided by VN-100 Rugged IMU running at 100 Hz and MTK3339 GPS module running at 10 Hz, respectively. The MES Algorithm 1 was developed in C++ using the Eigen C++ template library for linear algebra and the ROS framework. The parameters of the sensors were defined empirically based on the noise variance of each sensor.

The weighting matrices Q and R for the MJLS-based EKF were chosen as:

$$Q = \begin{bmatrix} Q_g & 0_{3 \times 3} & 0_{3 \times 3} & 0_{3 \times 3} \\ 0_{3 \times 3} & Q_{b_g} & 0_{3 \times 3} & 0_{3 \times 3} \\ 0_{3 \times 3} & 0_{3 \times 3} & Q_a & 0_{3 \times 3} \\ 0_{3 \times 3} & 0_{3 \times 3} & 0_{3 \times 3} & Q_{b_a} \end{bmatrix}, \quad (30)$$

$$R_{\Theta} = \begin{bmatrix} R_m^{\theta 1} & 0_{3 \times 3} & 0_{3 \times 3} \\ 0_{3 \times 3} & R_a^{\theta 2} & 0_{3 \times 3} \\ 0_{3 \times 3} & 0_{3 \times 3} & R_p^{\theta 3} \end{bmatrix}, \quad (31)$$

where  $\theta 1 = \{M, VSO, NS\}$ ;  $\theta 2 = \{A, NS\}$ ;  $\theta 3 = \{GP, VSP, NS\}$ ;  $Q_g, Q_{b_g}, Q_a, Q_{b_a}, R_m^M, R_m^{VSO}, R_a^A, R_p^{GP}$  and  $R_p^{VSP}$  are covariances matrices, and the matrices  $R_m^{NS}, R_a^{NS}$  and  $R_p^{NS}$  are set with the previous Markov state values, since their values are cancelled in the EKF calculation.

The parameters of the scale estimation defined in Section III-A are set as  $\alpha = 0.75$  and  $n = 9$ . The thresholds to define the reliable and available sensors in Section III-B are set as  $\rho_m = 0.05$ ,  $\rho_a = 0.05$  and  $\rho_p = 12$ . Only the coordinates  $x$  and  $y$  were considered in the computation of (18).

Results obtained for outdoors navigation, on the sidewalk of a park, are shown in Figures 3-7. In Fig. 3 the trajectory is depicted, as estimated by the VSLAM and GPS module individually and by the proposed Markovian estimation system. The Markov states jumps during this experiment are presented in Fig. 4, where we can see that the system starts in Markov state M-G-GP; at around 70s it jumps to VSO-G-GP, because VSLAM orientation is available; at around 160s it jumps to VSO-G-VSP, since VSLAM position is available; at around 230s it jumps to VSO-G-GPS, because VSLAM is not reliable; and at around 295s it jumps again to VSO-G-VSP, once VSLAM becomes reliable. Small jumps also happen in seemingly random intervals due to changes in sensor availability and reliability, as shown in Fig. 7(c).

Details of the orientation and position of the platform during this experiment are presented in Figures 5 and 6. The zoom in Figures 7(a) and 7(b) show that the

system is able to provide robust position and orientation estimates in intervals that others sensors are not available or reliable. Based on these results, we can safely assume that MES is a better option than VSLAM and GPS in isolation, and that the proposed technique is able to deal with unforeseen changes in sensor states that would pose a challenge for standard data fusion techniques.

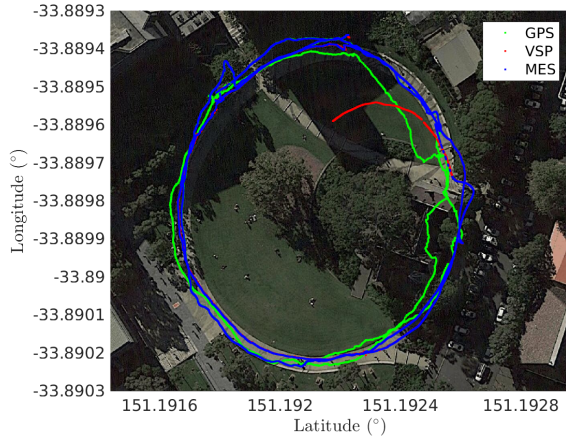


Fig. 3. Position estimation viewed on Google Earth.

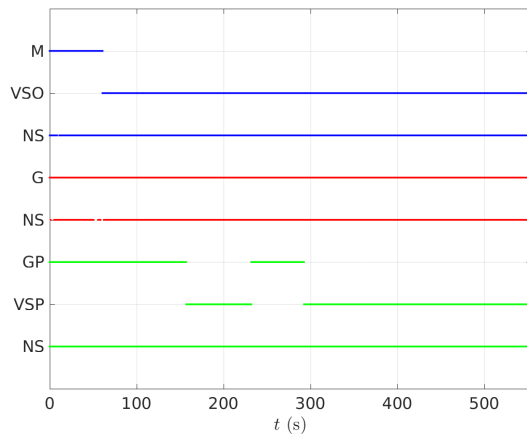


Fig. 4. Markov states transition during navigation.

## V. CONCLUSION

In this paper, we propose a Markovian Jump Linear Systems-based filtering for Visual and GPS aided inertial navigation system. MJLS is used to model the modes of operation of the navigation system. The MJLS-based EKF attempts to select the best mode of operation for determined time instant based on availability and reliability of each sensor. This is an improvement over the standard Kalman filter implementation, that uses information from all sensors simultaneously. Experimental results were performed on an outdoor environment considering the MES fusion of highly noisy data from an IMU, a monocular camera and a GPS module. Results show that MES consistently outperforms estimates from

each individual sensor, and the MJLS-based EKF is able to perform robust data fusion in challenging scenarios. Future work will integrate the MES framework developed with a 3D reconstruction system, to improve map generation quality.

## REFERENCES

- [1] A. Reid, F. Ramos, and S. Sukkarieh., “Bayesian fusion for multi-modal aerial images,” in *Robotics: Science and Systems*, (Berlin, Germany), 2013.
- [2] S. Owens, K. Sycara, , and P. Scerri, “Using immersive 3D terrain models for fusion of UAV surveillance imagery,” in *AIAA Infotech Aerospace Conference*, (Washington, USA), 2009.
- [3] H. Mayer and J. Bartelsen, “Automated 3D reconstruction of urban areas from networks of wide-baseline image sequences,” in *The International Archives of the Photogrametry, Remote Sensing and Spatial Information Sciences*, (Beijing, China), 2008.
- [4] T. Suzuki, Y. Amano, T. Hashizume, and S. Suzuki, “3D terrain reconstruction by small unmanned aerial vehicle using SIFT-based monocular SLAM,” *Journal of Robotics and Mechatronics*, vol. 23, no. 2, pp. 292–301, 2011.
- [5] S. Weiss, M. Achtelik, L. Kneip, D. Scaramuzza, and R. Siegwart, “Intuitive 3D maps for MAV terrain exploration and obstacle avoidance,” in *International Conference on Unmanned Aerial Vehicles*, 2010.
- [6] C. Forster, M. Pizzoli, and D. Scaramuzza, “SVO: Fast semi-direct monocular visual odometry,” in *IEEE International Conference on Robotics and Automation (ICRA)*, (Hong Kong, China), 2014.
- [7] R. Mur-Artal and J. D. Tardos, “Probabilistic semi-dense mapping from highly accurate feature-based monocular SLAM,” in *Robotics: Science and Systems Conference*, (Rome, Italy), 2015.
- [8] T. Schöps, J. Engel, and D. Cremers, “Semi-dense visual odometry for AR on a smartphone,” in *IEEE International Symposium on Mixed and Augmented Reality*, (Munich, Germany), 2014.
- [9] G. Klein and D. Murray, “Parallel tracking and mapping for small AR workspaces,” in *IEEE and ACM International Symposium on Mixed and Augmented Reality*, (Nara, Japan), 2007.
- [10] J. Engel, T. Schöps, and D. Cremers, “LSD-SLAM: Large-scale direct monocular SLAM,” in *European Conference on Computer Vision (ECCV)*, (Zurich, Switzerland), 2014.
- [11] G. Klein and D. Murray, “Parallel tracking and mapping on a camera phone,” in *IEEE International Symposium on Mixed and Augmented Reality (ISMAR)*, (Orlando, FL, USA), 2009.
- [12] M. Li, B. H. Kim, and A. Mourikis, “Real-time motion tracking on a cellphone using inertial sensing and a rolling-shutter camera,” in *IEEE International Conference on Robotics and Automation (ICRA)*, (Riverside, CA, USA), 2013.
- [13] P. Tanskanen, K. Kolev, L. Meier, F. Camposeco, O. Saurer, and M. Pollefeys, “Live metric 3D reconstruction on mobile phones,” in *IEEE International Conference on Computer Vision*, (Washington, DC, USA), 2013.
- [14] A. Concha, G. Loianno, V. Kumar, and J. Civera, “Visual-inertial direct SLAM,” in *IEEE International Conference on Robotics and Automation*, (Zaragoza, Spain), 2016.
- [15] M. Li and A. Mourikis, “Improving the accuracy of EKF-based visual-inertial odometry,” in *IEEE International Conference on Robotics and Automation (ICRA)*, (Saint Paul, MN, USA), 2012.
- [16] J. A. Hesch, K. Dimitrios G, S. L. Bowman, and Stergios, “Camera-IMU-based localization: Observability analysis and consistency improvement,” *The International Journal of Robotics Research*, vol. 33, no. 1, pp. 182–201, 2014.
- [17] J. A. Farrel, *Aided navigation GPS with high rate sensors*. New York: The McGraw-Hill Companies, 2008.

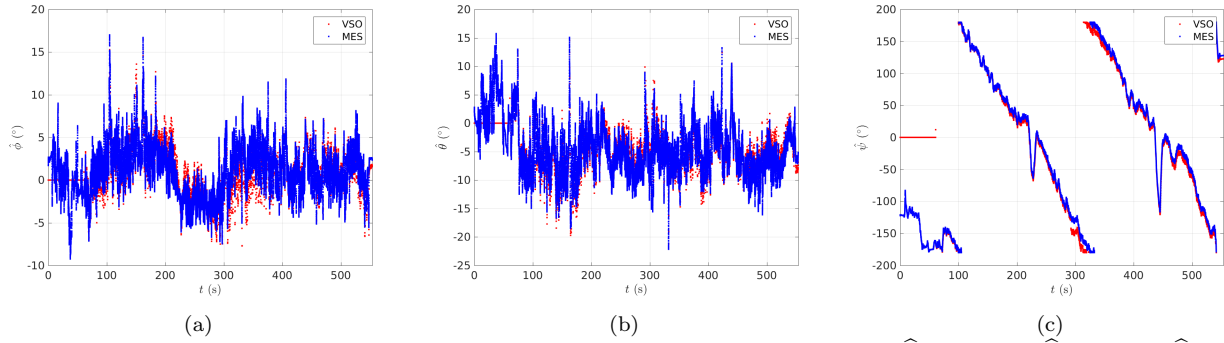


Fig. 5. MJLS-based EKF orientation estimation during the experiment: (a) Roll ( $\hat{\phi}$ ). (b) Pitch ( $\hat{\theta}$ ). (c) Yaw ( $\hat{\psi}$ )

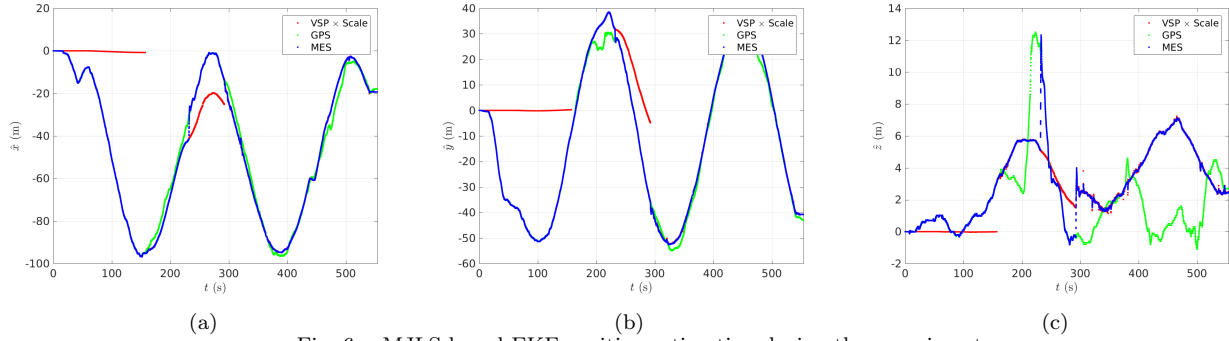


Fig. 6. MJLS-based EKF position estimation during the experiment.

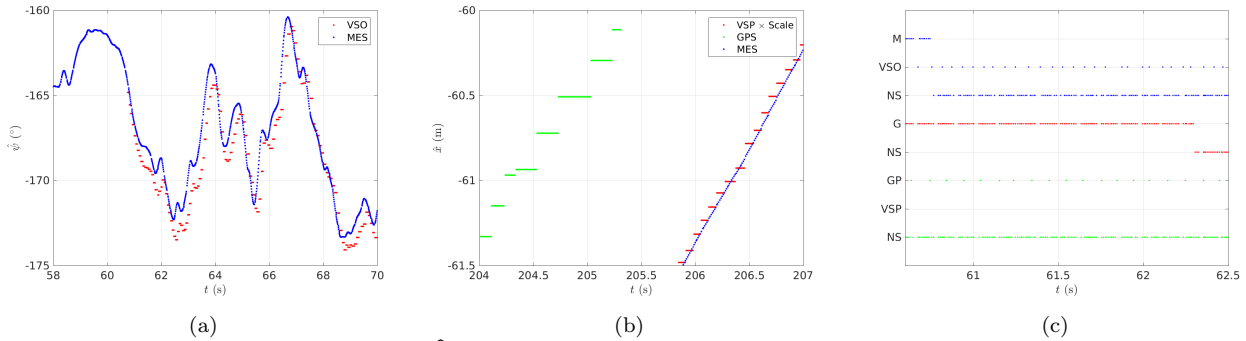


Fig. 7. (a) Zoom at the interval (58-70s) of  $\hat{\psi}$ . (b) Zoom at the interval (204-207s) of  $\hat{x}$ . (c) Zoom at the interval (60.5-62.5s) of the transitions of the Markov states  $\Theta$  during the experiment.

- [18] D. P. Shepard and T. E. Humphreys, "High-precision globally-referenced position and attitude via a fusion of visual SLAM, carrier-phase-based GPS, and inertial measurements," in *IEEE/ION Position, Location and Navigation Symposium - PLANS*, 2014.
- [19] D. Schleicher, L. M. Bergasa, M. O. a, R. Barea, and E. López, "Real-time hierarchical GPS aided visual SLAM on urban environments," *Journal of Field Robotics*, vol. 27, no. 5, pp. 609–631, 2010.
- [20] S. Lambrecht, S. L. Nogueira, M. Bortole, A. A. G. Siqueira, M. H. Terra, E. Rocon, and J. L. Pons, "Inertial sensor error reduction through calibration and sensor fusion," *Sensors*, vol. 16, no. 2, pp. 1–16, 2016.
- [21] S. L. Nogueira, S. Lambrecht, R. S. Inoue, M. Bortole, A. N. Montagnoli, J. C. Moreno, E. Rocon, M. H. Terra, A. A. G. Siqueira, and J. L. Pons, "Global Kalman filter approaches to estimate absolute angles of lower limb segments," *BioMedical Engineering OnLine*, vol. 16, pp. 1–20, 2017.
- [22] G. Q. de Jesus, R. S. Inoue, and M. H. Terra, "Information filtering and array algorithms for discrete-time Markovian jump linear systems subject to parametric uncertainties," *Information Sciences*, vol. 369, no. 1, pp. 287–303, 2016.
- [23] A. P. Gonçalves, A. R. Fioravanti, and J. C. Geromel, "Markov jump linear systems and filtering through network transmitted measurements," *Signal Processing*, vol. 90, no. 10, pp. 2842–2850, 2010.
- [24] O. L. V. Costa, M. D. Fragoso, and R. P. Marques, *Discrete-time Markov jump linear systems. Probability and its applications*. London: Springer, 2005.
- [25] Y. Yin, P. Shi, F. Liu, and K. L. Teo, "Filtering for discrete-time nonhomogeneous Markov jump systems with uncertainties," *Information Sciences*, vol. 259, no. 14, pp. 118–127, 2014.
- [26] Q. Zhong, J. Bai, B. Wen, S. Li, and F. Zhong, "Finite-time boundedness filtering for discrete-time Markovian jump system subject to partly unknown transition probabilities," *ISA Transactions*, vol. 53, no. 14, pp. 1107–1118, 2014.
- [27] N. Trawny and S. I., "Indirect Kalman filter for 3D attitude estimation," tech. rep., Dept. Of Computer Science & Engineering - University of Minnesota, 2005.
- [28] R. Mur-Artal, J. M. M. Montiel, and J. D. Tardós, "ORB-SLAM: a versatile and accurate monocular SLAM system," *IEEE Transactions on Robotics*, vol. 31, no. 5, pp. 1147–1163, 2015.